small methods
www.small-methods.com

Capturing and Quantifying Particle Transcytosis with Microphysiological Intestine-on-Chip Models

*Ludivine C. Delon, Matthew Faria, Zhengyang Jia, Stuart Johnston, Rachel Gibson, Clive A. Prestidge, and Benjamin Thierry**

Understanding the intestinal transport of particles is critical in several fields ranging from optimizing drug delivery systems to capturing health risks from the increased presence of nano- and micro-sized particles in human environment. While Caco-2 cell monolayers grown on permeable supports are the traditional in vitro model used to probe intestinal absorption of dissolved molecules, they fail to recapitulate the transcytotic activity of polarized enterocytes. Here, an intestine-on-chip model is combined with in silico modeling to demonstrate that the rate of particle transcytosis is ≈350× higher across Caco-2 cell monolayers exposed to fluid shear stress compared to Caco-2 cells in standard "static" configuration. This relates to profound phenotypical alterations and highly polarized state of cells grown under mechanical stimulation and it is shown that transcytosis in the microphysiological model is energy-dependent and involves both clathrin and macropinocytosis mediated endocytic pathways. Finally, it is demonstrated that the increased rate of transcytosis through cells exposed to flow is explained by a higher rate of internal particle transport (i.e., vesicular cellular trafficking and basolateral exocytosis), rather than a change in apical uptake (i.e., binding and endocytosis). Taken together, the findings have important implications for addressing research questions concerning intestinal transport of engineered and environmental particles.

1. Introduction

The intestinal epithelium performs essential physiological functions in the selective absorption of nutrients and antigens, and exclusion of microbiota and exogenous hazards including bacteria. The ability of intestinal epithelial cells to actively transcytose nano- and micron-sized particles has long been established, but the mechanisms and extent to which this process occurs in healthy intestinal tissues have been the object of significant discussion.[1] Specialized epithelial Microfold (M) cells located in the gut associated lymphoid tissue (GALT) have high particle transcytotic capabilities.[2] In addition to their role in shaping intestinal immune homeostasis, M cells have been postulated to play a key role in particle transport. However, they represent <1% of the cellular population in the human small intestine and while M cells may contribute to particle transport across the intestinal epithelium, several studies have shown that they are not essential to particle transport.[3–5] Conversely, there is strong evidence that nano- and micro-particles are efficiently transported across enterocytes in villi within the small intestine.[1,6–8] For example, Reineke et al. conclusively demonstrated in a rat model that non-phagocytic processes are key to the absorption of nano- and even micro-particles in the small intestine and, consequently, to their systemic bioavailability.[1] These studies refute the view that enterocyte transcytosis is a neglectable process in the small

L. C. Delon, Z. Jia, B. Thierry
Future Industries Institute
University of South Australia
Adelaide, SA 5095, Australia
E-mail: benjamin.thierry@unisa.edu.au
L. C. Delon, Z. Jia, C. A. Prestidge, B. Thierry
Clinical and Health Sciences
University of South Australia
Adelaide, SA 5000, Australia
M. Faria
Department of Biomedical Engineering
The University of Melbourne
Parkville, Victoria 3010, Australia
S. Johnston
School of Mathematics and Statistics
The University of Melbourne
Parkville, Victoria 3010, Australia
R. Gibson
School of Allied Health Science and Practice
Faculty of Health and Medical Sciences
University of Adelaide
Adelaide, SA 5050, Australia

The ORCID identification number(s) for the author(s) of this article can be found under https://doi.org/10.1002/smtd.202200989.

DOI: 10.1002/smtd.202200989

intestine, which is consistent with the fact that transcytosis is a hallmark of polarized epithelial cells.[9]

Better understanding of the intestinal uptake of nano- and micro-particles is directly relevant to human health. This is particularly time-critical considering the multiple recent reports of the near-ubiquitous presence of man-made particles, including nano and microplastics, within our environment, including the oceans.[10] Man-made colloids can rapidly enter food products, as illustrated recently in Scallop *Pecten maximus*,[11] and have even be found in human placenta.[12,13] Understanding and quantifying intestinal absorption is also critical for the development of effective oral formulations of drugs. This is important as oral delivery of biologically active molecules is the preferred route for drug administration.[14] Particle formulations can effectively protect their biological payloads from the harsh environment of the gastrointestinal tract, which is especially important for nucleic acids, peptides, and protein drugs/vaccines.[15] One of the requirements for the successful application of particle technology in oral drug delivery is their efficient absorption within the small intestine; and a lack of mechanistic insight into these processes has hampered the field.

A major bottleneck inhibiting the development of particle-based delivery systems has been the lack of in vitro models able to quantify and predict the intestinal absorption (uptake and transport) of particles.[16] Caco-2 cell monolayers grown within Transwell static permeable support are the most established in vitro model to evaluate the intestinal permeability and metabolism of molecules in dissolved states.[17] This is because the structural and functional differentiation of Caco-2 cell monolayers is somewhat similar to that exhibited by mature enterocytes. Robust correlations have been established between in vivo data and data obtained in Caco-2 cell monolayers.[18] However, Caco-2 cells cultured in static permeable support have extremely low rates of particle transcytosis.[19] While such assays are commonly used, there is little evidence demonstrating effective transport of particles within standard in vitro monoculture models based on Caco-2 cells.[20,21]

The superior biological representation offered by microfluidic organ-on-chip models over static ones is now well established.[22–24] These models offer the ability to apply biochemical and mechanical stimuli to cells within the microfluidic environment, which translates into distinctly different phenotypes and functions.[25–27] For example, Caco-2 cells cultured within intestine-on-chip (IOC) models differentiate into all cellular subtypes of the intestinal epithelium.[28,29] IOC models are increasingly employed to examine the effects of drugs, as well as for personalized medicine and disease modeling.[28,30,31] Surprisingly, to date there is no report on transport of particles in IOC, but only a single study reports semi-quantitatively on the transport of nanoparticles within an organ-on-chip model: Huh et al. report increased nanoparticle transport rates in a lung-on-chip model, in better agreement with the physiological situation.[32]

To establish the validity of IOC models in particle absorption studies, here we systematically investigate the uptake and transport of nanoparticles within a microfluidic IOC model. We demonstrate Caco-2 cells display efficient nanoparticle transcytosis in an IOC model, unlike when cultured in standard static permeable support models (350x increase). Importantly, rigorous quantification of the differences in transcytosis between these setups necessarily requires excluding the significant confounding experimental factors between the static and dynamic environments. We accomplish this by fitting our experimental data to a novel mathematical model that accounts for hydrodynamic differences and enables determination of the rates of particle transcytosis, apical uptake, and basolateral exocytosis. We demonstrate that the overall transcytosis rate is ≈900 fold higher in the IOC condition when compared to the static permeable support assay; and that this is largely explained by a ≈500 fold increase in basolateral exocytosis of particles. It is noteworthy that the rate of apical uptake is largely unchanged between these conditions. Finally, we investigate the mechanisms for this strikingly increased ability to transport nanoparticles by blocking specific uptake pathways. This is the first detailed investigation of the utility of IOC as models of the small intestine with respect to the intestinal uptake and transport of nanoparticles. Additionally, it demonstrates the value of kinetic modeling to extract quantitative parameters from complex organ-on-a-chip systems.

2. Results

2.1. Fluid Shear Stress Affects Morphology, Mucus Secretion, and Metabolism of Caco-2 Cell Monolayers

We have previously conducted a systematic study of the effect of fluid shear stress (FSS) on the phenotype and function of Caco-2 cells monolayers cultured on glass substrates within microfluidic devices with Hele–Shaw geometry.[33] Building on this data, we have now designed and established a microfluidic IOC model compatible with particle transport studies and characterized the Caco-2 cells monolayers grown for 5 days on porous polycarbonate membranes under shear stresses of 0.025 dyn.cm^{-2} (see **Figure 1**W). First, we demonstrate that the F-actin network displays a higher density in cells cultured in the IOC compared cells cultured for 21 days in the standard Transwell static permeable support model (Figure 1A,B). We then compare the secreted mucus in the two models. As illustrated in Figure 1C,D, increased Alcian blue staining is observed in the IOC compared to the static permeable support model, confirming increase in glycocalyx production. Mucin 2 is also stained and is almost entirely absent in the static permeable support. In contrast, in the IOC, Mucin 2 expression is more pronounced, though inhomogeneous that possibly result from washing-off of the extracellular mucus during necessary sample processing for immunostaining (Figure 1E,F). The thickness of the mucus layer is estimated to be up to 5 µm (Figure S1E, Supporting Information) and is in agreement with previous studies demonstrating microfluidic FSS drastically increases the secretion of mucus by Caco-2 cells.[29,34] As expected, apical expressions of tight junction proteins zona-occludens (ZO)-1 and occludin were elevated in the IOC (Figure 1Q–T; Figure S1C,D,F, Supporting Information), confirming the barrier integrity of the monolayers. Villin 1 expression is also increased on the apical membrane of cells in the microfluidic chamber and is up to 2 µm thick over the top of the cells (Figure 1G,H; Figure S1E, Supporting Information). This is in agreement with previous studies where it is shown that FSS

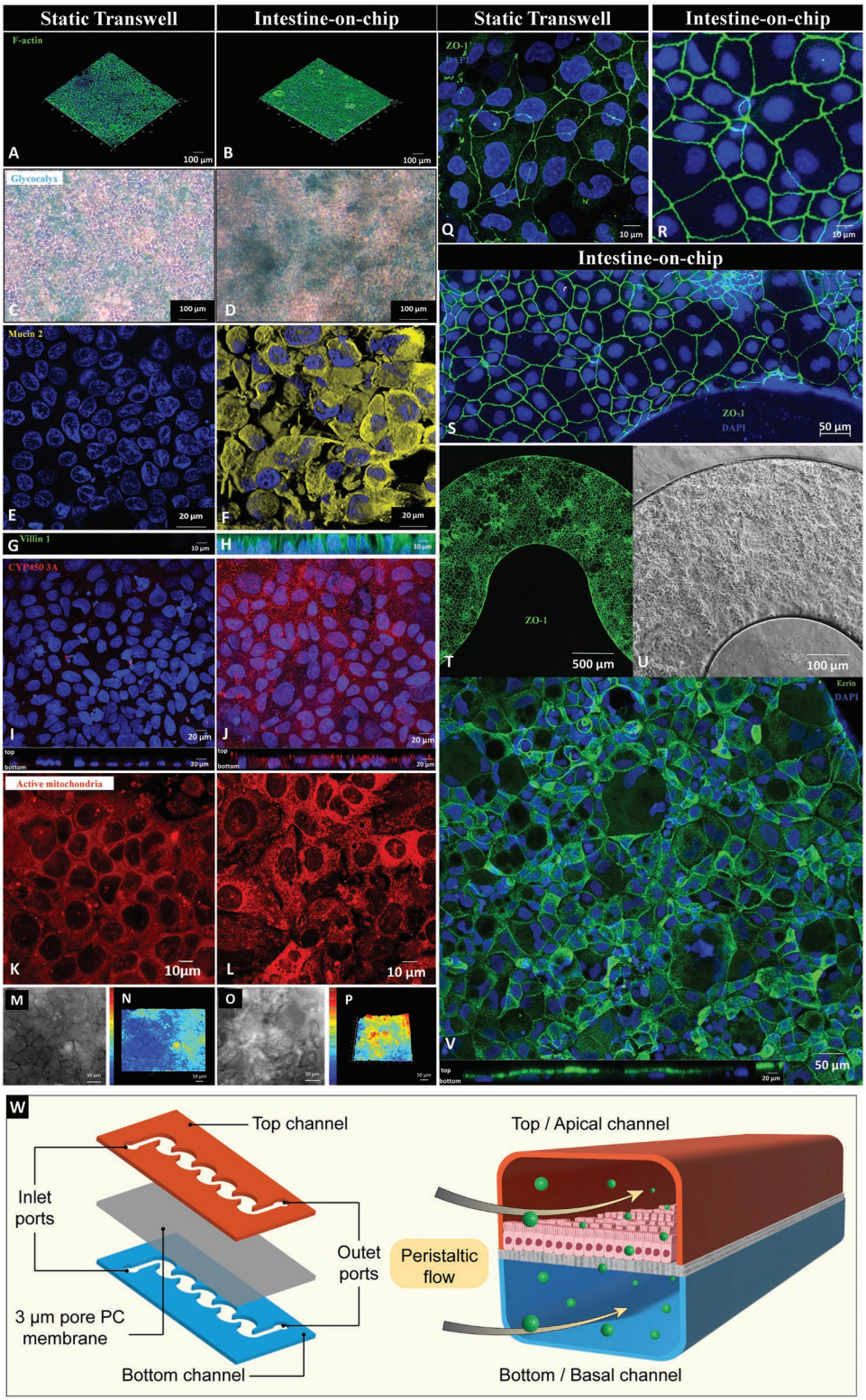

Figure 1. Effect of culture conditions on key characteristics and morphology of Caco-2 cell monolayers. Static culture (21 days) is shown in A, C, E, G, I, K, M, N, and Q, microfluidic IOC culture (5 days) in B, D, F, H, J, L, O, P, R, S, T, and V. A&B: 3D reconstructions (from z-stack) of confocal images displaying F-actin (green) and nuclei (blue) staining. C and D: Images from inverted microscope showing Alcian Blue staining for glycocalyx production. E and F: Confocal images (from z-stack) showing Muc-2 staining (yellow). G and H: Orthogonal projections of confocal images (from z-stack) showing villin 1 expression (green). I and J: Expression of the CYP450 3A4 (red). K and L: Confocal images (from z-stack) of active mitochondria (red) stained by Mitotracker Deep Red FM. M, N, O, and P: Digital holographic images of Caco-2 cells grown in static conditions for 21 days in static permeable

induces increased development of microvilli and a more dense network of F-actin.[31,35] We also demonstrate the expression of ezrin apically, which further confirms the polarization of Caco-2 cell monolayer in the IOC (Figure 1V). Next, we visualize the expression of the enzyme cytochrome (CYP) 450 3A4 and the presence of active mitochondria. CYP450 3A4 is primarily present on the apical surface of the cells and is markedly abundant in the monolayer grown in the IOC. In contrast, this enzyme is not expressed in the cells grown under static conditions in the static permeable support assay (Figure 1I,J). This suggests that drug metabolism may be improved in Caco-2 cells grown in dynamic versus static conditions.[36] However, further investigation of the effect of shear stress on the drug metabolism should be performed to ascertain the utility of IOC model in drug intestinal absorption studies. The mitochondrial activity (corresponding to higher mitochondrial membrane potential) is assessed by measuring the fluorescence intensity of Mitotracker Deep Red FM. Higher mitochondrial activity is observed in cells cultured in the IOC as compared to the population in the static permeable support (Figure 1K,L; Figure S1G,H, Supporting Information) that is confirmed by imaging flow cytometry (Figure S2, Supporting Information). Increased mitochondrial activity in Caco-2 cells cultured in the IOC may be associated with the changes in their tight junction proteins, as previously demonstrated.[37] Finally, we investigate the effect of FSS on the 3D structure/morphology of the cellular monolayer by using digital holography microscopy. We find that the Caco-2 cell monolayers display an increased and more irregular optical thickness when grown in IOC compared to static permeable support (Figure 1M–P). Multi-nucleated cells were occasionally observed in Caco-2 cells monolayers grown under fluid shear stress within the IOC (Figure S1F, Supporting Information). Altogether, this data confirm that the application of FSS within the microfluidic environment strongly influences the differentiation and polarization of Caco-2 cell monolayers compared to the static permeable support environment that lacks fluid flow and thus does not provide mechanical stimuli to the cells.

2.2. Nanoparticle Characterization and Surface Modification

The colloidal properties of the fluorescently labeled polystyrene (PS) nanoparticles used in this study were systematically assessed (Figure S3, Supporting Information). Aminated PS nanoparticles have a mean diameter of 200 nm with a narrow size distribution (PDI < 0.01) (Figure S3, Supporting Information) and zeta potential of +10 mV. Homo-bifunctional poly ethylene glycol (PEG) carboxylic acid (molecular weight of 2 kDa) is surface conjugated to the primary amines to coat the nanoparticles and increase their ability to transport through mucus as PEG coating significantly increases the mucus diffusion coefficient of nanoparticles.[38,39] The PEG content and density are optimized by varying the ratio of PS to PEG used in the preparation process.[40] Terminal carboxylic groups on the grafted PEG chains are further reacted using carbodiimide chemistry to bioconjugate the nanoparticles with Concanavalin A (Con A). Con A is a lectin with high binding affinity to enterocytes apical membranes and has been shown to improve particle transport through the intestinal epithelium.[40,41] The zeta potential of PEGylated particles and ConA-modified particles decreases to −7 and −23 mV, respectively (Figure S3, Supporting Information). The hydrodynamic diameter of the PEGylated and ConA particles increases compared to the aminated nanoparticles (from 235 to 251 and 271 nm, respectively, PDIs for both PEGylated and ConA particles were <0.01).

2.3. Transcellular Transport of Nanoparticles within Intestine-on-Chip Model

Having characterized the Caco-2 cell monolayers grown in both IOC and static permeable support, we next quantify their respective barrier integrity by measuring the transport rates of Lucifer Yellow (LY) and FITC-dextran 4 kDa (FD4). These small hydrophilic molecules primarily cross the intestinal epithelium via the paracellular route[42] and consequently their permeability varies depending on tight junction integrity and opening. Here, we refer to the apparent permeability P_{app} for transport of small tracer molecules, and to transcytosis rate t_r for the transport of particles. For the IOC, samples were collected from the outlet of the basal/lower channel every hour for 6 h. For the static permeable support, the basolateral solution was sampled every hour for 4 h (see SM-8 for more details). Experiments were repeated three times independently for each condition (see details in Experimental Section, SM-8). The apparent permeability coefficients P_{app} determined for Lucifer Yellow in both IOC and static permeable support are ≤12 nm s^{-1}, which indicates well-established Caco-2 cell monolayers.[43,44] The P_{app} for Lucifer Yellow in the IOC is significantly lower than in static permeable support (3 nm s^{-1} versus 10 nm s^{-1}, respectively; p-value = 0.007; **Figure 2**A), which is consistent with the observation that monolayers cultured within IOC display higher levels of tight junction markers. This is also consistent with previous studies reporting higher transepithelial electrical resistance (TEER) for monolayers within IOC compared to static permeable support.[30] We also measure the permeability for FD4 to further assess the paracellular transport in both models. P_{app} for FD4 is 14.8 nm s^{-1} +/− 0.94 in static permeable support and 3.8 nm s^{-1} +/−1.3 in IOC, (p = 0.005; Figure 2A). The P_{app} for FD4 in Caco-2 monolayers in Transwell has been previously reported to be in the range 0.2 to 10 nm s^{-1}.[45] This is a fairly broad range of values that may be related to differences in the experimental setup including the Caco-2 cells passage number (20–55). Nevertheless, our data conclusively show that the permeability coefficient for small molecules is lower for Caco-2 cell monolayers cultured within IOC than in static permeable support.

support (Static Transwell) (M,N) and in the IOC for 5 days under 0.02 dyn.cm^{-2} shear stress (O,P). Phase holograms (M,O), and reconstructed objects (N,P) are shown (scales indicate the optical thickness of cells). Q, R, S, and T: Confocal images (from z-stack) showing tight junctional protein ZO-1 (green) expressed in Caco-2 cell monolayers cultured in Static Transwell (Q) and in the IOC at different magnifications (R, S, and T). U: Phase contrast bright field image. V: Confocal image (from z-stack) showing ezrin (green) expressed in Caco-2 cell monolayer cultured in the IOC and orthogonal projection xy showing apical expression of ezrin. W: Schematic of Static Transwell versus IOC set-ups used for the culture of Caco-2 cell monolayers.

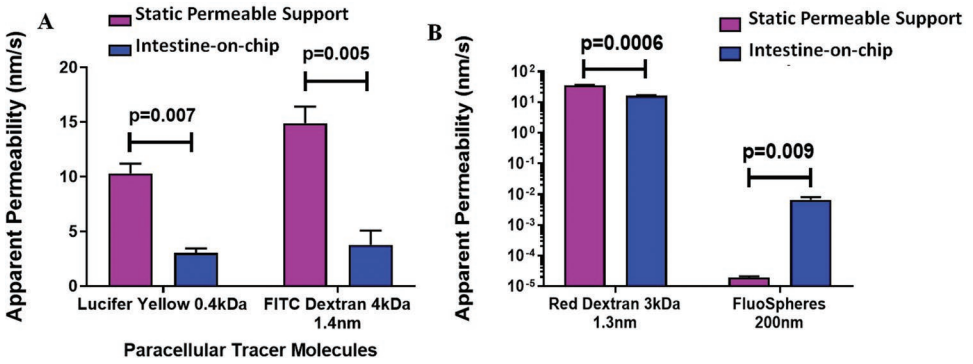

Figure 2. Effect of culture conditions on the permeability to small tracer molecules and on the transport of nanoparticles. A) Apparent permeabilities of Caco-2 monolayers for Lucifer Yellow and 4 kDa Dextran in static permeable support and in IOC (*t*-test, $n = 3$). B) Apparent permeabilities of Caco-2 monolayers for 3 kDa Dextran and 200 nm FluoSpheres in static permeable support and in IOC (*t*-test, $n = 3$).

Next, we investigate the transport of highly fluorescent PS nanoparticles across Caco-2 cells monolayers grown in the two models. We chose to use 200 nm particles as this size is often considered to be the upper limit for transcellular transport by enterocytes.[46] We determine that the 200 nm FluoSpheres nanoparticles are transported across the cellular monolayer to a much greater extent in the IOC compared to the static permeable support conditions. The rate of transport t_r is calculated (see experimental details) to be $\approx 2.00 \times 10^{-5}$ nm s^{-1} in static permeable support and ≈0.007 nm s^{-1} in IOC ($p = 0.009$), which represents an increase of ≈350x for the cells cultured in the microfluidic environment (Figure 2B). As a control, a transport experiment is performed with no cells grown in either IOC. As expected, a significant increase is measured in both cases when compared to IOC with intact cellular monolayers (≈10 000-fold increase, $p = 0.0004$, Figure S4, Supporting Information). To confirm the integrity of the Caco-2 cell monolayers during the nanoparticle transport studies, we perform the transport experiment simultaneously with rhodamine-labeled dextran 3 kDa (RD3). Similar to the data obtained for FD4 and Lucifer Yellow, RD3 has a significantly higher permeability in static permeable support than in IOC (P_{app}: 35.26 nm s^{-1} in static permeable support versus 15.95 nm s^{-1} in IOC, $p = 0.0006$). Importantly, the RD3 data confirm that the presence of the nanoparticles does not significantly damage Caco-2 cell monolayer paracellular barrier function in either model. This observation agrees with the previous report by Lamson et al. that only nanoparticles smaller than 100 nm affect paracellular barrier integrity.[47] The FluoSpheres data indicate that in the IOC, an average of 11 300 nanoparticles/h/cm^2 are transported, while only 31 nanoparticles/h/cm^2 are transported in static permeable support. The actual kinetics of transport are presented in Figure S5 (Supporting Information) and transport results summarized in Figure S6 (Supporting Information).

2.4. Experimental Effect of Flow Conditions during Transport Studies

Next we determine the effect of the presence of flow conditions on both sides of the porous polycarbonate membrane separating the two fluidic compartments of the IOC (**Figure 3**). The absence of flow on both sides of the membrane during the particle transport experiment ("Chip transport without flow") for monolayers grown for 5 days under fluid shear stress yielded a significant increase in transport in comparison to the situation when flow is present on both side of the membrane during the same particle transport experiment (t_r Chip even flow = 0.007 nm s^{-1} versus t_r "Chip transport without flow" = 0.09 nm s^{-1}; $p = 0.02$; Figure 3A). On the other hand, the P_{app} for the paracellular tracer RD3 dextran remains unchanged for the different flow conditions, which demonstrates the maintenance of monolayer integrities. Similarly, the uptake of the nanoparticles without flow during the particle incubation experiment in the IOC is increased, but not significantly (Figure S7, Supporting Information).

We also test the effect of applying a very low fluid shear stress, i.e., creating a "near-static" culture environment for the Caco-2 cells in the IOC ("Chip cells cultured with no shear stress"). Measurement for cells cultured within the IOC under fully static conditions could not be carried out due to its small volume and the need to regularly refresh the medium. Note that the actual transport experiment was in this case carried out under flow to allow for direct comparison. A significant decrease in the FluoSpheres t_r was measured for monolayers cultured under the "cells near-static" condition (t_r Chip "even flow" = 0.007 nm s^{-1} versus t_r 'Chip cells cultured with no shear stress' = 0.0006 nm s^{-1}; $p = 0.02$; Figure 3A), although it did not revert to the t_r measured in the static permeable support model.

2.5. Effect of Surface Modification of the Nanoparticles

To better understand the relevance of the IOC in regard to nanoparticle transport, we determine the transport rate of PEGylated and ConA-modified FluoSpheres nanoparticles using the approach detailed above for aminated FluoSpheres nanoparticles (Figure 3B). PEGylated FluoSpheres are transported across IOC-Caco-2 cell monolayers at 0.07 nm s^{-1}, which is higher than the transport rate measured for the aminated FluoSpheres nanoparticles (aminated FluoSpheres t_r = 0.007 nm s^{-1} versus PEGylated FluoSpheres t_r = 0.07 nm s^{-1}, $p = 0.06$). We also examine the effect of PEGylation of FluoSpheres on the uptake in the IOC, and observe a decrease in the uptake of PEGylated

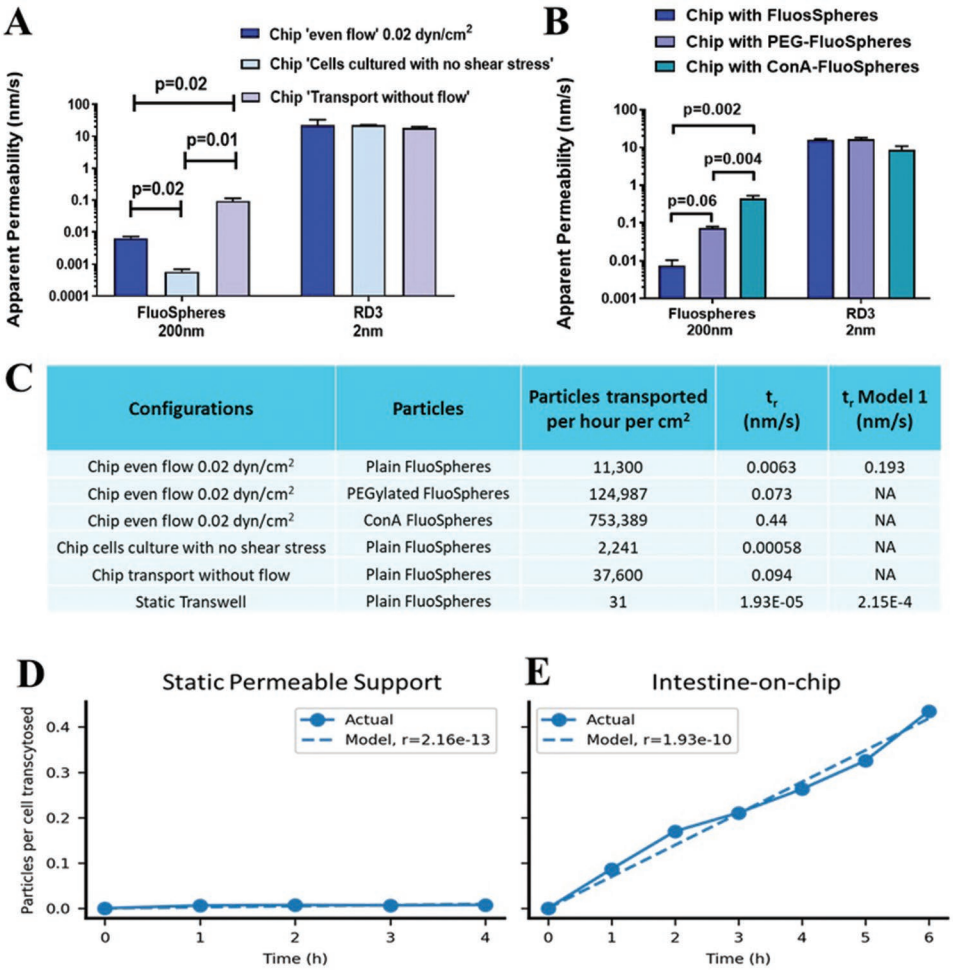

Configurations	Particles	Particles transported per hour per cm²	t_r (nm/s)	t_r Model 1 (nm/s)
Chip even flow 0.02 dyn/cm²	Plain FluoSpheres	11,300	0.0063	0.193
Chip even flow 0.02 dyn/cm²	PEGylated FluoSpheres	124,987	0.073	NA
Chip even flow 0.02 dyn/cm²	ConA FluoSpheres	753,389	0.44	NA
Chip cells culture with no shear stress	Plain FluoSpheres	2,241	0.00058	NA
Chip transport without flow	Plain FluoSpheres	37,600	0.094	NA
Static Transwell	Plain FluoSpheres	31	1.93E-05	2.15E-4

Figure 3. Effects of the flow conditions and nanoparticles coatings on FluoSpheres transport. A) Apparent permeabilities for FluoSpheres and 3 kDa Dextran in IOC measured in the absence of flow for Caco-2 cell monolayers grown for 5 days under flow condition ("Chip transport without flow") and measured in the presence of flow for monolayers grown under near-static conditions ("Chip cells cultured with no shear stress") (*t*-test, $n = 3$). B) Effect of PEG and Con A-PEG coatings of FluoSpheres on their apparent permeability within IOC (*t*-test, $n = 3$). C) Table summarizing the transport data with the different models. D,E) Experimental and fitted model for overall transcytosis.

FluoSpheres in the IOC compared to the static permeable support (at 2 h, $p = 0.03$) when the experiment is performed in the IOC (Figure S8, Supporting Information). However, we have previously demonstrated that the uptake of PEGylated silica particles increases in a single layer microchamber IOC.[34] In combination, this supports the fact that PEGylated particles are taken up and transcytosed at a higher rate by Caco-2 cells cultured in the two-chamber IOC. The rate of transport of the ConA-modified nanoparticles is also significantly higher than plain aminated FluoSpheres (aminated FluoSpheres $t_r = 0.007$ nm s^{-1} versus ConA FluoSpheres $t_r = 0.44$ nm s^{-1}, $p = 0.002$).

2.6. Modeling of the Transport Data to Obtain Objective Quantitative Transcytosis Rates

The experimental setups for IOC and static permeable support models are different in several notable ways relevant to transport studies. There are differences in: the introduction of the nanoparticle suspensions (continuously or once); whether particle sedimentation is a relevant phenomenon (no or yes); cell culture surface area; incubation dimensions; and the method of counting transcytosed particles.

To rigorously and quantitatively compare the transport of nanoparticles in these two cell culture systems, we develop and implement a mathematical model that accounts for these experimental differences. Analogous approaches have been used previously to better quantify cellular association.[48] Within this model, the transcytosis is represented as a linear process, i.e., the rate of particle transcytosis is proportional to the amount of nanoparticles the cells are exposed to. We fit this model with our experimental time-course data (see Experimental Section for more details) to obtain the transcytosis rate t_r (nm s^{-1}) for the two conditions. This approach can be used to accurately compare the biological processes controlling the transport of the nanoparticles in an experiment-independent manner. Strikingly, when taking into consideration these experimental

confounding factors, Caco-2 cells grown under the dynamic conditions of IOC are found to transcytose nanoparticles ≈900 times more than those grown within the static condition of the static permeable support. (Figure 3D,E)

2.7. Computational Model to Delineate Nanoparticle Absorption and Exocytosis

Transcytosis of nanoparticles across the Caco-2 cell epithelial monolayer can be considered as a two-step process. First, nanoparticles associate to cells (i.e., bind and are internalized). Second, cells exocytose nanoparticles into the basal compartment. We seek to determine which of these biological processes is up-regulated for Caco-2 cells cultured within the IOC microfluidic environment. To this end, we first measure the number of particles associated per cell in each of the two models over several time points (**Figure 4**A–C; Figure S9, Supporting Information). In both models, the number of nanoparticles associated to Caco-2 cells increases as a function of time. However, significantly more particles accumulate over time in static permeable support than in IOC (Figure S9, Supporting Information). There are two contrasting possible explanations for this. First, this observation could be explained by a higher rate of nanoparticle association with Caco-2 cells cultured in static permeable support. Alternatively, Caco-2 cells cultured within IOC may exocytose nanoparticles at a higher rate, either in the apical compartment or in the basal one. To investigate whether increased apical exocytosis can explain these differences, we culture Caco-2 cells under dynamic and static conditions on glass substrates to eliminate the possibility for basal exocytosis (similar to our previous study[34]). A significant decrease in the Caco-2 cells' apical exocytosis of FluoSpheres is measured for cells grown in IOC compared to static permeable support (measured as mean fluorescence intensity (MFI), Static MFI = 30 338 a.u. versus IOC MFI = 8119 a.u., $p = 0.0005$, Figure S10, Supporting Information).

To independently quantify the association and basal exocytosis rates, we fit both the association and transcytosis data to a "two stage" computational model in which particles first associate with cells in the apical compartment and are then eventually transcytosed to the basal compartment (see Experimental Section). As in Section 5.11., this computational modeling approach fully accounts for experimental differences and allows direct, quantitative comparison between experiments done in different perfusion conditions. Using this model, we calculate an association rate a_r and a basal exocytosis rate b_r for each time course experiment. Interestingly, the association rate a_r was remarkably similar for both conditions (6.23 nm s^{-1} versus 6.60 nm s^{-1} in IOC and in static permeable support, respectively; Figure 4D,E). However, the basal exocytosis rate b_r is substantially different; it is more than 500 times higher for IOC than static permeable support models (0.98 and 0.0022 nm s^{-1}, respectively; Figure 4F,G).

2.8. Biological Mechanisms of Nanoparticles Endocytosis and Transcytosis in Intestine-on-Chip

Finally, to understand the endocytic mechanisms by which nanoparticles are internalized and transported across Caco-2 cell monolayers cultured in IOC, we conducted a series of experiments using a panel of pharmacological inhibitors that suppress specific endocytic pathways. Prior to the use of inhibitors,

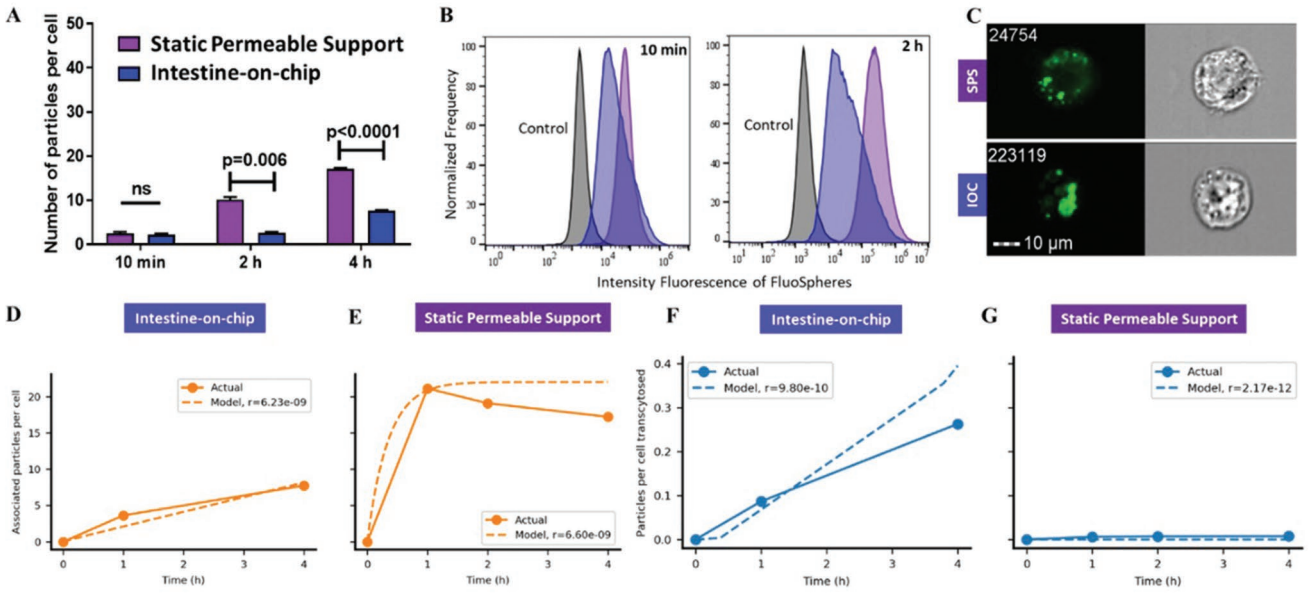

Figure 4. Effect of FSS on the uptake/association in/to cells of FluoSpheres. A) Number of FluoSpheres nanoparticles per cell over time in static permeable support versus IOC (Welch two-tailed *t*-test, $n = 3$). B) Normalized FITC intensity graphs at the 10 min and 2 h time-points. C) Images of FluoSpheres uptaken by Caco-2 cells cultured in static permeable support (top row) and in IOC (bottom row) (Channel 2: Alexa Fluor 488, Channel 4: brightfield). Experimental data and fitted "two stage" model for D,E) uptake and F,G) total trancytosis for monolayers grown in IOC and static permeable support.

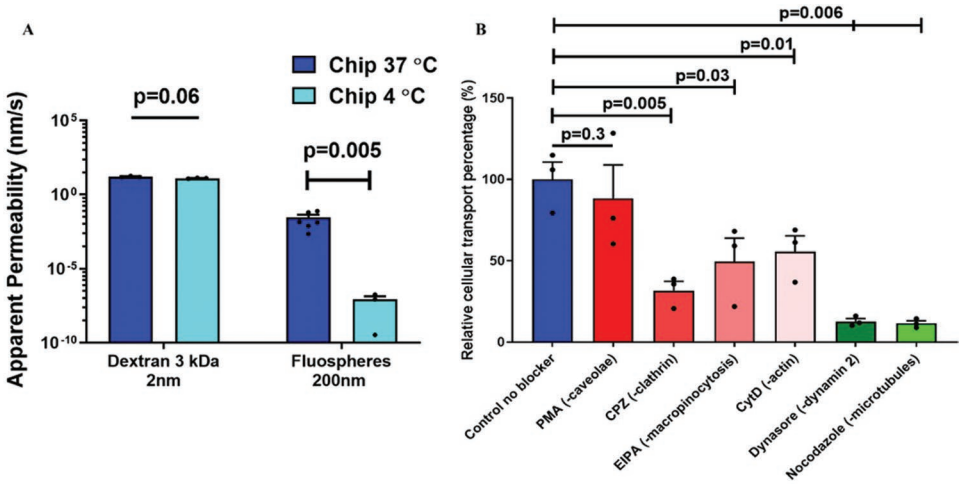

Figure 5. Effect of temperatures and endocytic blockers on nanoparticles uptake/association and transport in Caco-2 cells cultured in IOC. A) Apparent permeability for FluoSpheres and 3 kDa Dextran for cells cultured at either 37 or at 4 °C (two-tailed Mann–Whitney test, $n > 3$). B) Relative percentage of FluoSpheres transport in presence of endocytic blockers ($n = 3$). Values were compared to the untreated control using *t*-test.

we aim to verify if the transcytosis activity observed is mediated by energy-dependent processes. To this end, the cellular transport of FluoSpheres at 37 and 4 °C are measured as presented in **Figure 5**A. Permeability in the IOC to RD3 is mostly unchanged at 4 °C, which confirms the conservation of barrier integrity. However, conducting the experiment at 4 °C significantly decreases the transport of the FluoSpheres nanoparticles (≈99% reduction versus 37 °C, $p = 0.02$) indicating that the transport is an active, energy-dependent phenomenon carried out by the cells cultured under FSS conditions. The uptake as determined by imaging flow cytometry is also significantly decreased when cells are exposed to nanoparticles at 4 °C ($p = 0.009$, Figure S11, Supporting Information).

Various endocytic inhibitors were then used to further ascertain the cellular mechanisms underpinning the vast increase in nanoparticle transcytosis in Caco-2 cell monolayers cultured within IOC. Here, we show the percentage of transport of FluoSpheres relative to the control (i.e., exposed to particles but not treated with blockers) after blocking caveolae (phorbol-12-myristate-13-acetate – PMA), clathrin (chlorpromazine hydrochloride – CPZ), macropinocytosis (N-(ethyl-N-isopropyl)-amiloride – EIPA) pathways, and actin polymerization (Cytochalasin D – CytD). CPZ, EIPA and CytD all cause statistically significant decreases in the transport of particles as summarized in Figure 5. Blocking of the clathrin pathway with CPZ reduces the transport 68% compared to the untreated control. The decreases are 50% with EIPA and 45% with CytD. Treatment with PMA does not induce a significant decrease (12%) in transport.

To provide a more comprehensive view of the transport process, we also determine the effect of blocking these pathways on the association/uptake of the nanoparticles to/in cells using imaging flow cytometry. Treatment with CPZ and EIPA triggers the largest reduction in nanoparticle uptake (77%, $p = 0.003$ and 80%, $p = 0.003$, respectively), followed by CytD (≈54% of decrease, $p = 0.03$) (Figures S11 and S12, Supporting Information). Confocal images qualitatively confirm the imaging flow cytometry data (Figures S11 and S12, Supporting Information). Together, these results show co-mediation of clathrin-mediated pathway and macropinocytosis, which indicates the variety and non-specificity of nanoparticles endocytosis and transcytosis by Caco-2 cells cultured in the IOC. Most importantly, the results demonstrate that non-phagocytic (endocytosis) processes by polarized enterocytes are responsible for uptake and transport of FluoSpheres in the Caco-2-IOC model. Finally, to fully ascertain the transcytosis of nanoparticles by Caco-2 cells in the IOC, blockers of vesicular trafficking were tested. Dynasore, a blocker of the GTPase activity of dynamin and hence dynamin-dependent endocytosis in cells[49] leads to a significant decrease in nanoparticles transport (87% compared to untreated control; $p = 0.006$; Figure 5B). Similarly, disruption of microtubules with nocodazole significantly suppresses the transport of nanoparticles across the cells (decrease by 88%; $p = 0.006$; Figure 5B). The effects of dynasore and nocodazole indicate a major involvement of the transcellular vesicular trafficking in the overall nanoparticle transport across the Caco-2 cell monolayers cultured in the IOC.

3. Discussion

The passage of particles across the intestinal epithelium has been reported to occur by different pathways, namely transcytosis through either polarized enterocytes[1,6,50] or M cells located in the GALT,[51] and to much lesser extent by paracellular transport (tight junctions opening),[52,53] by persorption, i.e., through gaps at the villous tip following loss or renewal of enterocytes,[54] and more hypothetically through migratory macrophages and phagocytes.[55] As noted by Reineke et al. and others in mice and rat models, nano and sub-micron particles are mostly transported by the absorptive epithelium rather than in the Peyer's patches of the ileum.[1,6,56] In vivo and even ex vivo mechanistic studies are non-trivial to perform due to the complexity and heterogeneity of the intestinal epithelium. In addition, while animal models remain the gold standard method to obtain insights on the bioavailability and biodistribution of

orally administrated nanoparticles, quantitative insights on the intestinal uptake, and transport of nano- and micro-particles are difficult to extract. Moreover, animal studies suffer from noteworthy limitations, including well-known inter-species differences and existence of many confounding factors such as animals' age, physiological and nutritional status, and the microbiome.

These challenges highlight the need for in vitro models that recapitulate the physiological transcytotic competency of enterocytes in the small intestine. While Caco-2 cell monolayers grown in static permeable support have been widely used in drug intestinal absorption studies and generally correlate well with in vivo data for molecules in solute states, they display only limited transport of colloids.[20,21] For the first time, we provide both qualitative and quantitative confirmation that nanoparticles are actively transcytosed by the absorptive Caco-2 cells cultured within an IOC model. We employ computational simulations to fit the experimental data. The results obtained from the computational model reveal that the increased transport within IOC results from a significantly higher rate of nanoparticle basal exocytosis (500 fold) by the Caco-2 cells rather than from increased particle uptake. This explanation could not be distinguished from other potential explanations without the computational model, and highlights the importance of in silico models to tease out complex biological processes and eliminate the confounding factors associated with experimental set-ups.

The nanoparticle transport assay is carried out simultaneously with low molecular weight rhodamine-labeled dextran to ensure the integrity of the cellular monolayer. This provides a reliable quality control method to ensure the suitability of all tested IOCs prior to the start of the FluoSpheres nanoparticles (yellow-green fluorescence) transport experiment. The dextran data also confirm that Caco-2 cell monolayers cultured within IOC display higher barrier resistance to paracellular transport than when cultured in static conditions within static permeable support (Figure 2A). This is in agreement with previous studies[57,58] as well as with the high levels of expression of tight junctional proteins in IOC models as observed here (Figure 1) and previously reported.[33,59] The combination of these results suggests IOC models might not be well suited to study the intestinal absorption of soluble low molecular weight and hydrophilic molecules as they likely underestimate the permeability compared to the human intestinal epithelium in vivo.[18,60,61] Importantly, the simultaneous measurements of the FluoSpheres and LMW Dextran transport demonstrate that the 200 nm nanoparticles used here, either in the aminated, PEGylated, or Con A bioconjugated form, have no significant effect on the barrier integrity of the cellular monolayer, although a modest increase in the paracellular transport of Dextran was measured. The preservation of the integrity of the paracellular function of the Caco-2 monolayers in presence of the nanoparticles is supported by the fact that ≈99% of the transport was inhibited at 4 °C. This observation is in agreement with recent in vivo data reported by Lamson et al. in their systematic investigation of the effect of nanoparticle physicochemical characteristics on the paracellular barrier integrity and transport of low molecular weight macromolecules, such as dextran, as only particles smaller than 100 nm were found to moderately affect paracellular transport.[62]

The large increase in nanoparticle transport mediated by Caco-2 cells basal exocytosis in IOC can be somewhat compared to the previous report by Huh et al. in which both lung epithelial and endothelial cells cultured within microfluidic devices display 4 times increased rates of nanoparticles translocation across the alveolar-capillary interface compared to static permeable support.[32] Although in this study the cells are mechanically stimulated by the application of 10% mechanical strain rather than by FSS, this confirms transcytotic capabilities of epithelial monolayers are strongly influenced by mechanobiological stimulation. As noted above, while several studies have confirmed that particles can be transported through the intestinal epithelium to achieve systemic circulation, most reports are qualitative. Available quantitative studies are usually focused on measuring intestinal absorption, and in vivo data are scarce on nanoparticle transport rate through the epithelium. However, Jani et al. reported significant systemic availability for PS microspheres administrated orally for 10 days to female Sprague Dawley rats with extents ranging from 7% (1 μm particles) to up to 34% (50 nm nanoparticles) of the administered dose, depending on the particle size and other experimental parameters.[63] Our previous ex vivo microscopic study showed that ≈3% of 200 nm latex nanoparticles taken-up by the epithelium are transported into the lamina propria within 4 h.[40]

Based on these considerations and our experimental findings, we advocate that Caco-2 cells-IOCs have the potential to serve as a much-needed in vitro model of the small intestine for studies investigating the transport of colloids across the epithelium. This is not an entirely surprising finding as, on one hand transcytosis is an inherent characteristic of polarized epithelial cells, and on the other hand, it is now well established that dynamic culture conditions enhance the polarization of epithelial cells and alter their structure, function, phenotype and response to treatments compared to static conditions. For example, in the present report as well as our previous systematic study of the effect of the FSS, we find a significant increase in mitochondrial and potentially drug metabolism activity for Caco-2 cells within the IOC.[33] The dramatic influence of the microfluidic environment on Caco-2 cell phenotype was also shown in recent transcriptomic studies.[26,27] Heterogeneous phenotypes regarding cell cycles, differentiation, and intestinal functions including digestion, absorption, drug transport, and metabolism of xenobiotics were observed. It is also noteworthy that increased mitochondria biogenesis was observed in Caco-2 cells cultured in the IOC compared to the static permeable support culture. This observation agrees with several studies reporting increased mitochondrial biogenesis in vivo in response to fluid shear stress.[64] Mitochondrial function is a very important aspect of intestinal cell differentiation and function as well as intestinal homeostasis.[65] The increased transcytotic potential of cells cultured in the IOC might be linked to this increased mitochondrial activity and this question warrants further investigation.

The application of FSS also leads the Caco-2 cells to secrete mucus, which is typically not the case for static culture. Interestingly, the presence of mucus within the IOC does not hamper the FluoSpheres particle transport, although it may contribute to the lower rates of uptake compared to monolayers on static permeable support. The introduction of a muco-penetrating

PEG coating on the surface of the FluoSpheres nanoparticles leads to a further increase in both particle uptake and transport, in agreement with our previous study in a one-layer IOC model.[35] It is however important to note that the mucus layer present within Caco-2 cells based-IOC differs in several important ways to the mucus found in intestinal mucosa. First, it is of much lower thickness and somewhat inhomogeneous, and as such its ability to serve as an efficient physical barrier function is unclear. Second, intestinal mucus has a highly dynamic structure that is constantly and rapidly produced that might even produce a hydrophobic driving force "pushing" particles toward the intestinal epithelium and away from the aqueous lumen.[1] Further bioconjugation of the PEGylated nanoparticles with the lectin Con A leads to a further increase in the rates of uptake and transport, presumably due to efficient binding of ConA to enterocytes.[41] This demonstrates the feasibility of using IOC to objectively screen for biointerfacial engineering of particles aimed at increasing intestinal absorption.

Finally, we investigate the endocytic mechanisms underlying the nanoparticles transport within the IOC. Transport studies conducted at 4 °C almost completely inhibit nanoparticles transport within the IOC while having no effect on the paracellular transport of low-molecular weight dextran. As a common pathway, clathrin-mediated endocytosis is often involved in the internalization of extracellular macromolecules and nanoparticles, and it can be inhibited by CPZ.[66,67] CPZ significantly reduces both the absorption and transport of the FluoSpheres nanoparticles, directly demonstrating the function of this pathway.[68] In addition, particles can be internalized via macropinocytosis by ruffling plasma membrane to form cargo-loaded macropinosomes.[69] Macropinocytosis has been previously demonstrated to be a main endocytic mechanism employed by Caco-2 cells to transport large iron (Fe)-binding protein.[70] In addition, previous studies on HeLa cells show that EIPA inhibits the uptake of positively charged, 113 nm diameter nanoparticles.[71] CytD is also partly an inhibitor of macropinocytosis and phagocytosis as it is inducing depolymerization of actin that is essential in this pathway.[72] Inhibiting macropinocytosis with EIPA and CytD leads to a decrease in nanoparticle uptake and transport, confirming the involvement of this pathway. Caveolae can bud off from the membrane to form caveosome, resulting in the endocytosis of extracellular content.[73–75] Based on the inhibition of the caveolae mediated pathway with PMA, it is however clear that the observed transport of FluoSpheres is not mediated by caveolae.

While abundant literature exists describing the various cellular pathways of nanoparticles uptake,[76,77] limited data are available for enterocytes in vivo. Molecular pathways of endocytosis depend strongly on the size of the particle, and also on their biointerfacial properties. Reineke et al. report that 200 and 500 nm carboxylated particles can be observed in cytosolic vesicles in the rat small intestine and that the uptake of 500 nm and 1 μm particles is mediated via clathrin-mediated endocytosis in combination with macropinocytosis and potentially phagocytosis.[1] Although we only investigate one size of nanoparticles, which is a limitation of the present study, our data are in good general agreement with the data available in animal models, and supports the use of IOC models for nanoparticle transport studies.[46] Further investigation of the transport of nanoparticles with different size, shape, and composition is warranted to further correlate the IOC model with existing ex vivo and in vivo data. While a liquid–liquid cell culture microfluidic configuration is used in the present study, a further refinement of the method should investigate the feasibility of transitioning to air–liquid culture once priming of the cellular monolayer by culture under fluid shear stress is completed. This would significantly broaden the scope of microphysiological models.

4. Conclusion

In vivo animal models have significant limitations as evidenced by the paucity of quantitative studies. On the other hand, current in vitro models based on static culture in static permeable support display very little nanoparticle transport, and as such do not recapitulate the levels of transcytosis observed in vivo. We demonstrate that monolayers of the commonly used absorptive Caco-2 cell line cultured within IOC have significantly increased rates of transcytosis compared to monolayers cultured within static permeable support. Through the application of a computational model, we conclude that this striking finding is due to a massive increase in basal exocytosis of absorbed particles, rather than in the rate of particle uptake. Mechanistic studies reveal the involvement of clathrin-mediated endocytosis and macropinocytosis as well as a major involvement of the transcellular vesicular trafficking pathways, which is in conceptual agreement with the highly polarized nature of cells grown under fluid shear stress in microphysiological systems. While it is difficult due to the lack of data to quantitatively benchmark the uptake and transport data obtained within the IOC with in vivo data, we anticipate that IOC will become a mainstay approach to assess intestinal absorption and this work serves as a template for how to accomplish this for nano-carrier systems.

5. Experimental Section

Nanoparticles used in the study had been characterized by DLS. PDMS microfluidic chips were fabricated using soft lithography protocols. Caco-2 cells were cultured in DMEM medium with 10% FBS and 1% P/S for 5 days in the different microfluidic chips, their differentiation was characterized and compared to static Caco-2 cell cultures. Cell permeability assays to small molecules and nanoparticles were performed simultaneously based on fluorescence measurement and verified with endocytosis blockers, endocytosis, and exocytosis assays. Computational modeling using partial and ordinary differential equations enables to better quantify both uptake and transport of the particles. A detailed description of materials and methods is provided in SM-9 Appendix, Materials and Methods.

Code Availability: The git clone code used to objectively and quantitatively compare the transcytosis between static permeable support assays and IOC assays is freely available at https://bitbucket.org/mwfcomp/cell_particle_kinetic_models.git git checkout 0f177f9.

Supporting Information

Supporting Information is available from the Wiley Online Library or from the author.

Acknowledgements

The authors acknowledge funding from the Australian Research Council Linkage grant LP150100032. This work was performed in part at the South Australian node of the Australian National Fabrication Facility under the National Collaborative Research Infrastructure Strategy to provide nano and microfabrication facilities for Australia's researchers. The authors also thank Dr. Chia-Chi Chien for assisting in the fabrication of the PMMA slabs of the IOC, and Dr. Zhaobin Guo for performing the Digital Holographic Microscopy. This work was supported by a gift from the estate of Réjane Louise Langlois.

Open access publishing facilitated by University of South Australia, as part of the Wiley - University of South Australia agreement via the Council of Australian University Librarians.

Conflict of Interest

The authors declare no conflict of interest.

Author Contributions

L.D. conceived and designed the transport study in the static and microfluidic models. L.D. planned and performed the biological experiments, the chip development and fabrication, and analyzed the data all under the supervision of R.G., C.P., and B.T. Z.J. was responsible for modification and characterization of polystyrene aminated particles for the uptake and transport studies. M.F. and S.J designed and performed the in silico analysis. L.D. and M.F. led the data analysis for generation of figures as well as assembly of the manuscript. L.D., M.F., and B.T. wrote the manuscript and supporting information. Z.J., S.J., R.G., and C.P. were responsible for overseeing the entire effort, including preparation of the manuscript.

Data Availability Statement

The data that support the findings of this study are available from the corresponding author upon reasonable request.

Keywords

cellular transcytosis, enterocytes, intestinal absorption, intestine-on-chip

Received: July 29, 2022
Revised: November 2, 2022
Published online: December 22, 2022

[1] J. J. Reineke, D. Y. Cho, Y.-T. Dingle, A. P. Morello, J. Jacob, C. G. Thanos, E. Mathiowitz, *Proc. Natl. Acad. Sci. USA* **2013**, *110*, 13803.
[2] H. Ohno, *J. Biochem.* **2016**, *159*, 151.
[3] K. E. Carr, R. A. Hazzard, S. Reid, G. M. Hodges, *Pharm. Res.* **1996**, *13*, 1205.
[4] G. M. Hodges, E. A. Carr, R. A. Hazzard, K. E. Carr, *Dig. Dis. Sci.* **1995**, *40*, 967.
[5] J. Limpanussorn, L. Simon, A. D. Dayan, *J. Pharm. Pharmacol.* **1998**, *50*, 745.
[6] E. Sanders, C. T. Ashworth, *Exp. Cell Res.* **1961**, *22*, 137.
[7] P. U. Jani, A. T. Florence, D. E. McCarthy, *Int. J. Pharm.* **1992**, *84*, 245.
[8] S. H. Smyth, S. Feldhaus, U. Schumacher, K. E. Carr, *Int. J. Pharm.* **2008**, *346*, 109.
[9] M. D. Garcia-Castillo, D. J.-F. Chinnapen, W. I. Lencer, *Cold Spring Harb Perspect. Biol.* **2017**, *9*, a027912.
[10] B. Giese, F. Klaessig, B. Park, R. Kaegi, M. Steinfeldt, H. Wigger, A. von Gleich, F. Gottschalk, *Sci. Rep.* **2018**, *8*, 1565.
[11] M. Al-Sid-Cheikh, S. J. Rowland, K. Stevenson, C. Rouleau, T. B. Henry, R. C. Thompson, *Environ. Sci. Technol.* **2018**, *52*, 14480.
[12] H. Bové, E. Bongaerts, E. Slenders, E. M. Bijnens, N. D. Saenen, W. Gyselaers, P. Van Eyken, M. Plusquin, M. B. J. Roeffaers, M. Ameloot, T. S. Nawrot, *Nat. Commun.* **2019**, *10*, 3866.
[13] A. Ragusa, A. Svelato, C. Santacroce, P. Catalano, V. Notarstefano, O. Carnevali, F. Papa, M. C. A. Rongioletti, F. Baiocco, S. Draghi, E. D'Amore, D. Rinaldo, M. Matta, E. Giorgini, *Environ. Int.* **2021**, *146*, 106274.
[14] A. A. Date, J. Hanes, L. M. Ensign, *J. Control. Release* **2016**, *240*, 504.
[15] E. Fattal, N. Tsapis, *Clin. Transl. Imaging* **2014**, *2*, 77.
[16] E. Moroz, S. Matoori, J.-C. Leroux, *Adv. Drug Delivery Rev.* **2016**, *101*, 108.
[17] A. Fedi, C. Vitale, G. Ponschin, S. Ayehunie, M. Fato, S. Scaglione, *J. Control. Release* **2021**, *335*, 247.
[18] S. Yee, *Pharm. Res.* **1997**, *14*, 763.
[19] A. M. Bannunah, D. Vllasaliu, J. Lord, S. Stolnik, *Mol. Pharm.* **2014**, *11*, 4363.
[20] B. He, P. Lin, Z. Jia, W. Du, W. Qu, L. Yuan, W. Dai, H. Zhang, X. Wang, J. Wang, X. Zhang, Q. Zhang, *Biomaterials* **2013**, *34*, 6082.
[21] A. Beloqui, D. J. Brayden, P. Artursson, V. Préat, A. des Rieux, *Nat. Protoc.* **2017**, *12*, 1387.
[22] B. Zhang, A. Korolj, B. F. L. Lai, M. Radisic, *Nat. Rev. Mater.* **2018**, *3*, 257.
[23] E. W. Esch, A. Bahinski, D. Huh, *Nat. Rev. Drug Discovery* **2015**, *14*, 248.
[24] D. E. Ingber, *Adv. Sci.* **2020**, *7*, 2002030.
[25] C. L. Thompson, S. Fu, H. K. Heywood, M. M. Knight, S. D. Thorpe, *Front Bioeng. Biotechnol.* **2020**, *8*, 1426.
[26] K. Kulthong, G. J. E. J. Hooiveld, L. Duivenvoorde, I. Miro Estruch, V. Marin, M. van der Zande, H. Bouwmeester, *Sci. Rep.* **2021**, *11*, 3234.
[27] W. Shin, Z. Su, S. S. Yi, H. J. Kim, Single-Cell Transcriptomics Elucidates in Vitro Reprogramming of Human Intestinal Epithelium Cultured in a Physiodynamic Gut-on-a-Chip. *bioRxiv* **2021**.
[28] A. Bein, W. Shin, S. Jalili-Firoozinezhad, M. H. Park, A. Sontheimer-Phelps, A. Tovaglieri, A. Chalkiadaki, H. J. Kim, D. E. Ingber, *Cell Mol. Gastroenterol. Hepatol.* **2018**, *5*, 659.
[29] H. J. Kim, D. E. Ingber, *Integr. Biol.* **2013**, *5*, 1130.
[30] H. J. Kim, D. Huh, G. Hamilton, D. E. Ingber, *Lab Chip* **2012**, *12*, 2165.
[31] R. Villenave, S. Q. Wales, T. Hamkins-Indik, E. Papafragkou, J. C. Weaver, T. C. Ferrante, A. Bahinski, C. A. Elkins, M. Kulka, D. E. Ingber, *PLoS One* **2017**, *12*, e0169412.
[32] D. Huh, B. D. Matthews, A. Mammoto, M. Montoya-Zavala, H. Y. Hsin, D. E. Ingber, *Science* **2010**, *328*, 1662.
[33] L. C. Delon, Z. Guo, A. Oszmiana, C.-C. Chien, R. Gibson, C. Prestidge, B. Thierry, *Biomaterials* **2019**, *225*, 119521.
[34] K. Pocock, L. C. Delon, A. Khatri, C. Prestidge, R. Gibson, C. Barbe, B. Thierry, *Biomater. Sci.* **2019**, *7*, 2410.
[35] K. Pocock, L. Delon, V. Bala, S. Rao, C. Priest, C. Prestidge, B. Thierry, *ACS Biomater. Sci. Eng.* **2017**, *3*, 951.
[36] I. F. Sevrioukova, T. L. Poulos, *Dalton Trans.* **2013**, *42*, 3116.
[37] L. M. JanssenDuijghuijsen, S. Grefte, V. C. J. de Boer, L. Zeper, D. A. M. van Dartel, I. van der Stelt, M. Bekkenkamp-Grovenstein, K. van Norren, H. J. Wichers, J. Keijer, *Front Physiol.* **2017**, *8*, 794.
[38] J. Palacio, N. A. Agudelo, B. L. Lopez, *Curr. Opin. Chem. Eng.* **2016**, *11*, 14.
[39] M. Yang, S. K. Lai, T. Yu, Y.-Y. Wang, C. Happe, W. Zhong, M. Zhang, A. Anonuevo, C. Fridley, A. Hung, J. Fu, J. Hanes, *J. Control. Release* **2014**, *192*, 202.

[40] Z. Jia, A. Wignall, L. Delon, Z. Guo, C. Prestidge, B. Thierry, *ACS Biomater. Sci. Eng.* **2021**, https://doi.org/10.1021/acsbiomaterials.0c01355.
[41] B. Devriendt, B. G. De Geest, B. M. Goddeeris, E. Cox, *J. Control. Release* **2012**, *160*, 431.
[42] Y. Jin, Y. Takegahara, Y. Sugawara, T. Matsumura, Y. Fujinaga, *Microbiology* **2009**, *155*, 35.
[43] *Nat. Rev. Drug Discovery* **2010**, *9*, 215.
[44] C.-M. Lehr, in *In Vitro Test Systems for Drug Absorption and Delivery*, CRC Press, Florida, USA **2002**.
[45] S. H. Kim, M. Chi, B. Yi, S. H. Kim, S. Oh, Y. Kim, S. Park, J. H. Sung, *Integr. Biol.* **2014**, *6*, 1122.
[46] L. Delon, R. J. Gibson, C. A. Prestidge, B. Thierry, *J. Control. Release* **2022**, *343*, 584.
[47] N. G. Lamson, A. Berger, K. C. Fein, K. A. Whitehead, *Nat. Biomed. Eng.* **2020**, *4*, 84.
[48] M. Faria, K. F. Noi, Q. Dai, M. Björnmalm, S. T. Johnston, K. Kempe, F. Caruso, E. J. Crampin, *J. Control. Release* **2019**, *307*, 355.
[49] E. Macia, M. Ehrlich, R. Massol, E. Boucrot, C. Brunner, T. Kirchhausen, *Dev. Cell* **2006**, *10*, 839.
[50] J. Kreuter, U. Müller, K. Munz, *Int. J. Pharm.* **1989**, *55*, 39.
[51] P. U. Jani, D. E. McCarthy, A. T. Florence, *Int. J. Pharm.* **1992**, *86*, 239.
[52] K. E. Carr, S. H. Smyth, M. T. McCullough, J. F. Morris, S. M. Moyes, *Prog. Histochem. Cytochem.* **2012**, *46*, 185.
[53] M. Aprahamian, C. Michel, W. Humbert, J. P. Devissaguet, C. Damge, *Biol. Cell* **1987**, *61*, 69.
[54] G. Volkheimer, in Old Herborn University Seminar Monograph, Herborn Litterae, **2001**, p. *7*.
[55] M. E. LeFevre, R. Olivo, J. W. Vanderhoff, D. D. Joel, *Proc. Soc. Exp. Biol. Med.* **1978**, *159*, 298.
[56] J. Rejman, V. Oberle, I. S. Zuhorn, D. Hoekstra, *Biochem. J.* **2004**, *377*, 159.
[57] M. Chi, B. Yi, S. Oh, D.-J. Park, J. H. Sung, S. Park, *Biomed. Microdevices* **2015**, *17*, 58.
[58] H.-Y. Tan, S. Trier, U. L. Rahbek, M. Dufva, J. P. Kutter, T. L. Andresen, *PLoS One* **2018**, *13*, e0197101.
[59] G. J. Feldman, J. M. Mullin, M. P. Ryan, *Adv. Drug Delivery Rev.* **2005**, *57*, 883.
[60] A. Avdeef, K. Y. Tam, *J. Med. Chem.* **2010**, *53*, 3566.
[61] H. Lennernäs, K. Palm, U. Fagerholm, P. Artursson, *Int. J. Pharm.* **1996**, *127*, 103.
[62] N. G. Lamson, A. Berger, K. C. Fein, K. A. Whitehead, *Nat. Biomed. Eng.* **2020**, *4*, 84.
[63] P. Jani, G. W. Halbert, J. Langridge, A. T. Florence, *J. Pharm. Pharmacol.* **1990**, *42*, 821.
[64] C. Miceli, F. Roccio, L. Penalva-Mousset, E. Morel, P. Codogno, N. Dupont, *Autophagy* **2020**, *16*, 2287.
[65] E. Rath, A. Moschetta, D. Haller, *Nat. Rev. Gastroenterol. Hepatol.* **2018**, *15*, 497.
[66] W. J. Atwood, *J. Neurovirol.* **2001**, *7*, 307.
[67] Y. Okamoto, H. Ninomiya, S. Miwa, T. Masaki, *J. Biol. Chem.* **2000**, *275*, 6439.
[68] A. I. Ivanov, A. Nusrat, C. A. Parkos, *Mol. Biol. Cell* **2004**, *15*, 176.
[69] M. C. Kerr, R. D. Teasdale, *Traffic* **2009**, *10*, 364.
[70] S. Kalgaonkar, B. Lönnerdal, *J. Nutr. Biochem.* **2009**, *20*, 304.
[71] J. Dausend, A. Musyanovych, M. Dass, P. Walther, H. Schrezenmeier, K. Landfester, V. Mailänder, *Macromol. Biosci.* **2008**, *8*, 1135.
[72] S. Gold, P. Monaghan, P. Mertens, T. Jackson, *PLoS One* **2010**, *5*, e11360.
[73] B. Nichols, *J. Cell Sci.* **2003**, *116*, 4707.
[74] R. G. Parton, B. Joggerst, K. Simons, *J. Cell Biol.* **1994**, *127*, 1199.
[75] E. Smart, D. Foster, Y. Ying, B. Kamen, R. Anderson, *J. Cell Biol.* **1994**, *124*, 307.
[76] L. Kou, J. Sun, Y. Zhai, Z. He, *Asian J. Pharm. Sci.* **2013**, *8*, 1.
[77] R. A. Petros, J. M. DeSimone, *Nat. Rev. Drug Discovery* **2010**, *9*, 615.